Available online at www.sciencedirect.com
ScienceDirect
Microporous and Mesoporous Materials 110 (2008) 250–259
MICROPOROUS AND MESOPOROUS MATERIALS
www.elsevier.com/locate/micromeso

Adsorption of Pb^{2+}, Cu^{2+} and Cd^{2+} in FDU-1 silica and FDU-1 silica modified with humic acid

L.C. Cides da Silva [a], L.B.O. dos Santos [a], G. Abate [d], I.C. Cosentino [c], M.C.A. Fantini [b], J.C. Masini [a], J.R. Matos [a,*,1]

[a] Departamento de Química Fundamental, Instituto de Química, Universidade de São Paulo-USP, C.P. 66083, São Paulo, SP, Brazil
[b] Departamento de Física Aplicada, Instituto de Física, USP, CP 66318, 053-970 São Paulo, SP, Brazil
[c] Instituto de pesquisas energéticas e nucleares- IPEN – Av Prof. Lineu Prestes, 2242 São Paulo, SP, Brazil
[d] Departamento de Química, Universidade Federal do Paraná, CP 1901, CEP 81631-990, Curitiba-Pr, Brazil

Received 17 January 2007; received in revised form 7 June 2007; accepted 11 June 2007
Available online 14 June 2007

Abstract

Ordered mesoporous silica with cubic structure, type FDU-1, was synthesized under strong acid media using B-50-6600 poly(ethylene oxide)–poly(butilene oxide)–poly(ethylene oxide) triblock copolymer ($EO_{39}BO_{47}EO_{39}$) and tetraethyl orthosilicate (TEOS). Humic acid (HA) was modified to the synthesis process at a concentration of 1.5 mmol per gram of SiO_2. Thermogravimetry, small angle X-ray diffraction, nitrogen adsorption and high resolution transmission electron microscopy were used to characterize the samples. The pristine FDU-1 and FDU-1 with incorporated 1.5 mmol of HA were tested for adsorption of Pb^{2+}, Cu^{2+} and Cd^{2+} in aqueous solution. Incorporation of humic acid into the FDU-1 silica afforded an adsorbent with strong affinity for Cd^{2+}, Cu^{2+} and Pb^{2+} from single ion solutions. Adsorption of Cu^{2+} was significantly enhanced after incorporation of humic acid, a fact that can be explained by the formation of complexes with carboxylic and phenolic groups at low concentrations of the metal cation. The results demonstrated the potential applicability of FDU-1 with incorporated HA in the removal of low concentrations of heavy metal cations from aqueous solution, such as wastewaters, after usual precipitation of metal hydroxides in alkaline medium and proper pH conditioning in the range between 6 and 7.

Keywords: FDU-1 silica; Ordered mesoporous; Humic acid; SIA system; Wastewater; Heavy metal cation

1. Introduction

Since the discovery of surfactant-templated synthesis of ordered mesoporous materials (OMMs) [1–4], the research on the preparation and characterization of these novel nanostructured materials has been expanded very fast [5–12].

Among OMMs with different framework compositions, ordered mesoporous silicas (OMSs) are far the most investigated. Thousands of scientific papers were published within a little more than a decade dealing with synthesis, characterization and application of these materials. OMSs can be synthesized using a variety of procedures, including cost-effective ones. They have attractive properties such as high specific surface area, large mesopore volume, adjustable pore diameter, narrow pore size distribution, and adjusted surface properties. Moreover, several types of periodic porous structures are readily achievable for these materials. OMSs are useful for numerous applications as catalysts or catalyst supports, adsorbents, support for chromatographic packing, media for immobilization of biomolecules, components of sensors and adsorbents [5–17]. Highly ordered cubic cage-like mesoporous silica, named FDU-1, is synthesized from tetraethyl orthosilicate (TEOS) in the presence of poly(ethylene oxide)–poly(butylene

* Corresponding author. Tel.: +55 11 3091 3837x238; fax: +55 1 3091 3837x237.
E-mail address: jdrmatos@gmail.com (J.R. Matos).
[1] Tel.: +55 11 3091 2166; fax: +55 11 3091 2187.

1387-1811/$ - see front matter © 2007 Elsevier Inc. All rights reserved.
doi:10.1016/j.micromeso.2007.06.008

oxide)–poly(ethylene oxide) triblock copolymer (PEO–PBO–PEO) in a strong acidic media [18,19]. FDU-1 has a BET surface area of about 740 $m^2 g^{-1}$, a large pore size (ca. 12 nm), pore volume of 0.8 $cm^3 g^{-1}$ and wall thickness between 2.9 and 7.4 nm. Its exceptionally high thermal and hydrothermal stability can be attributed to the combination of its large wall thickness and the continuous 3-dimensional nature of its thick wall backbone [20]. Matos et al. [21] showed that FDU-1 is not a cubic Im3 m structure, as reported earlier, but a cubic *Fm3m* structure with a 3-D hexagonal intergrowth, similar to SBA-2 and SBA-12. It was demonstrated that the temperature and time control during the synthesis allow to gradually change the cage-like pores of FDU-1 to a highly open and accessible porous system with a narrow pore width distribution [18–21]. The preparation process requires hydrothermal treatment, which can be performed with a conventional microwave oven [22].

The present work uses the FDU-1 modified with HA to test the performance of the material as metal ion adsorbent. Humic substances (HS) are divided into three groups according to their solubility: humic acid, which is soluble in alkali and precipitate in acidic medium; fulvic acid, which is soluble in acidic or basic media; and humin, which is insoluble in the entire pH range [23]. Because of the high content of carboxylic and phenolic groups, HS interact strongly with pollutants such as heavy metals cations and pesticides, influencing their mobility and bioavailability in the environment [23]. In addition, they are able to form aggregates with mineral particles, enhancing adsorption or complexation of heavy metal ions [24]. Thus, the investigation of HS behavior in mineral phases has been widely carried out [25], especially in terms of the removal of water contaminants.

Lai et al. [26] demonstrated that a goethite-coated sand removes Cd^{2+} efficiently above pH 6, but at lower pH this process was almost negligible. However, the modification of this mineral phase with HA led to a significant increase in the adsorption capacity even at pH close to 2.5. Incorporation of humic acid increased the heterogeneity of adsorption sites because of the presence of carboxylic, phenolic and amine groups in its structure, increasing the adsorption of metal ions by surface complexation mechanism, even at low pH [26]. Moreover, the removal of Cd^{2+} was more efficient by goethite-coated sand, which was initially modified with HA, than that of the unmodified mineral exposed to a solution containing HA–Cd^{2+} complex ions. Liu and Gonzales [27] studied the removal of Cu^{2+}, Pb^{2+} and Cd^{2+} by montmorillonite (MT) in the presence and absence of humic acid (HA). This study showed that the presence of bivalent heavy metal cations increases adsorption of HA. Also, the presence of HA enhanced adsorption of these metal ions on MT, forming metal bridges between MT and HA.

Silva et al. [17] studied the synthesis of FDU-1 silica modified with humic acid performed with a microwave oven and its application for adsorption of Cd^{2+} in aqueous solution. This study showed that the incorporation of HA in walls of FDU-1 silica conferred to the material an excellent adsorption capacity for cadmium ions. In the present work, the use of FDU-1 functionalized with humic acid to adsorb other ions was checked against the pristine silica mesoporous material.

2. Experimental

2.1. Humic acid preparation

Fifteen grams of sodium salt of HA from Aldrich were dissolved in 100 mL of 0.1 M NaOH solution under N_2 atmosphere. After 15 min the suspension was centrifuged at 1000 rpm for 30 min and the supernatant phase was acidified with 6 M HCl until pH 1.0. The suspension was centrifuged and the precipitated HA was washed with deionized water four times for the removal of salt excess. Finally, the solid phase that consisted of HA was re-suspended in 250 mL of deionized water. The HA concentration in this stock suspension was 28.0 ± 0.6 g L^{-1}, which was determined gravimetrically by drying 1.00 mL aliquots. The ash content was (8.0 ± 0.5)% and the elemental composition of the dry HA was: (49.7 ± 0.1)% C, (4.3 ± 0.1)% H and (0.65 ± 0.02)% N determined by using the elemental analyzer 2400 instrument from Perkin Elmer. To facilitate the handling of the HA suspension, and its subsequent incorporation in FDU-1, the pH of a 25.00 mL aliquot was adjusted to 7.5 using 1.0 M $NaHCO_3$ solution followed by its dilution to 50.00 mL, which gave the final HA concentration of 14.0 g L^{-1}.

2.2. FDU-1 and FDU-1/HA_{15} synthesis

The synthesis of the FDU-1 samples was carried out using the same synthesis gel composition as reported by Yu et al. and Matos et al [18,19,21]: 1 TEOS: 0.00735 B50-6600: 6 HCl: 155 H_2O, where TEOS stands for tetraethylorthosilicate from Aldrich Chemical Company, B50-6600 is a poly(ethylene oxide)–poly(butylene oxide)–poly(ethylene oxide) triblock copolymer $EO_{39}BO_{47}EO_{39}$ from Dow Chemicals. In the synthesis of FDU-1/HA_{15}, 1.5 mmol of HA per gram of SiO_2 was used to obtain the sample. The mole number of HA was computed from its mean molar mass of 3000 Da, which was estimated from gel permeation chromatography [28]. In a typical synthesis procedure, 2 g of B50-6600 copolymer was dissolved in 120 g of 2 M HCl and stirred at room temperature until a homogeneous mixture was obtained. Subsequently, 8.32 g of TEOS, 34.3 mL of 14 g L^{-1} HA solution, respectively, were added. The resulting mixture was vigorously stirred in an open beaker for 24 h at room temperature. The precipitation was observed in 30–40 min after the addition of TEOS and HA solution. The obtained mixture was transferred into a Teflon vessel and heated under autogenous pressure for 120 min at 100 °C using a microwave oven. The microwave treatment was performed using

Microsynth Labstation for microwave assisted synthesis (Milestone Inc). Finally, the precipitate was filtered out, washed with ethanol and dried at 25 °C. The template inside the as-synthesized samples was removed by soxhlet extraction at boiling point for 12 h using ethanol to yield FDU-1/HA_{15} and FDU-1. The pure silica samples are denoted as FDU-1, whereas the HA modified materials are denoted as FDU-1/HA_{15} (15 represents concentration of HA in the synthesis gel, respectively, 1.5 mmol). The samples were named "AS", denoting the as-synthesized state with copolymer (and HA) inside the pores and named "EX", after template extraction.

2.3. Thermogravimetry

TG/DTG curves were obtained with a thermobalance model TGA 50 (Shimadzu) in the temperature range 25–900 °C, using platinum crucibles with ~3 mg of samples, under dynamic nitrogen atmosphere (50 mL min^{-1}) and heating rate of 10 °C min^{-1}.

2.4. Small angle X-ray diffraction (SAXRD)

The SAXRD experiments were carried out in a rotating anode X-ray generator (Rigaku), operating at 10 kW. The wavelength of the copper monochromatic X-ray beam was $\lambda = 1.5418$ Å. An image plate detector was utilized to record the scattering intensity as a function of the scattering vector, $q = (4\pi\sin\theta)/\lambda$, θ being half the scattering angle. The intensity was recorded during 2 h. The line focus geometry was used and the system was collimated by slits. A vacuum path between the sample and the detector was utilized. The scattering of the sample's holder was subtracted from the total measured intensities. The sample detector distance (~480 mm) was chosen in order to record the scattering for q values ranging from 0.008 $Å^{-1}$ to 0.35 $Å^{-1}$. The samples were placed inside a quartz tube, 2 mm in diameter.

2.5. Adsorption isotherms

Adsorption isotherms were measured with Micromeritics ASAP 2010 volumetric adsorption analyzer using nitrogen of 99.998% purity. Measurements were performed in the range of relative pressure from 10^{-6} to 0.99 liquid nitrogen on the samples degassed for 2 h, under vacuum of about 10^{-3} Torr, at 110 °C. The degassing temperature (110 °C) was selected to avoid the decomposition of attached organic ligands and ensure thermodecomposition of physically adsorbed water. The specific surface area was evaluated using BET method [29]. The total pore volume was estimated from the amount adsorbed at the relative pressure of 0.99. The pore size distribution (PSD) was calculated using BJH algorithm [30], with the relation between the capillary condensation pressure and the pore diameter established by Kruk, Jaroniec and Sayari (KJS) [31].

2.6. Structural and textural parameters obtained from nitrogen adsorption and small angle X-ray diffraction (SAXRD)

The pore diameter (W_d) was calculated using a geometrical equation proposed by Ravikovitch and Neimark [32] for materials with fcc structure:

$$W_d = a\left(\frac{6\varepsilon_{me}}{\pi v}\right)^{1/3}$$

where a is the unit-cell parameter, v is the number of spherical pores per unit cell ($v = 4$ for the fcc structure) and ε_{me} is the volume fraction of ordered mesoporous in the structure:

$$\varepsilon_{me} = \left(\frac{\rho V_p}{1 + \rho(V_p + V_m)}\right)$$

where ρ is the pore wall density, assumed to be equal to 2.2 g cm^{-3}, which is typical of amorphous silicas frameworks, V_p is the total primary mesopore volume and V_m is the micropore volume, both obtained from the N_2 adsorption data. The average pore wall thickness b in the fcc structure is determined as:

$$b = \frac{W_d(1 - \varepsilon_{me})}{3\varepsilon_{me}}$$

2.7. Highly resolution transmission electron microscopy (HRTEM)

For HRTEM observation, the samples were studied using a JEM-3010 (Cs 0.6 mm, resolution 0.17 nm) at 300 kV. HRTEM images were recorded with a slow scan CCD (Gatan 794). The FDU-1 samples were dispersed in isopropyl alcohol and put onto a carbon film deposited on a 400 mesh Cu grid.

2.8. Automated voltammetric measurements

Voltammetric measurements were carried out using an EG&G PAR model 263A potentiostat. An EG&G PAR model 303A Static Mercury Drop Electrode (SMDE) was used as working electrode, filled with purified and doubly distilled mercury. The flow cell adapted to the Hg capillary was already described in the literature [23] and the Hg drop radius used was 0.46 mm. The electrochemical cell was completed with an Ag/AgCl reference electrode (KCl saturated) and a platinum auxiliary electrode. Ultrapure N_2 ($O_2 < 2$ ppm) was used to remove dissolved O_2 from the solutions and to provide an inert atmosphere inside the cell.

A FIAlab 3500 (FIAlab Instruments, USA, Bellevue, WA) instrument was used in all experiments in the sequential injection mode according to Fig. 1. Solutions were driven by a 5.00 mL syringe pump and an eight port rotary valve, RV (Valco Instrument Co., Houston, TX). The

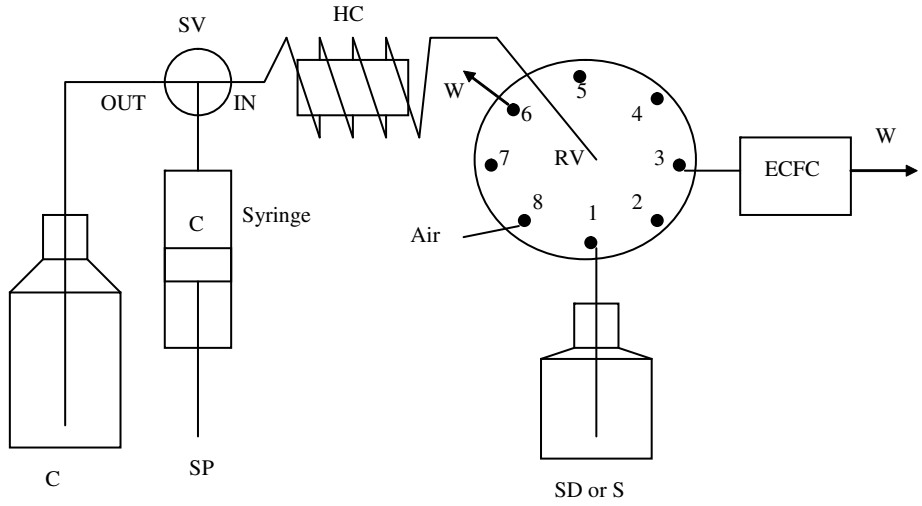

Fig. 1. Sequential injection manifold to automate the square wave anodic stripping voltammetry determination of Cd^{2+}, Pb^{2+} and Cu^{2+}. C = carrier (50 mmol L^{-1} acetic acid–sodium acetate buffer with pH 4.7 in 0.20 mol L^{-1} KCl); SV = syringe valve; SP = syringe pump; HC = holding coil (made of 3 m of PTFE tubing of 0.8 mm internal diameter); RV = eight port rotary selection valve; SD or S = standard or sample reservoir; ECFC = electrochemical flow cell (connection between ECFC and RV is made of 0.27 m of PTFE tubing of 0.5 mm i.d.); W = waste. More details about the ECFC are given in Ref. [23].

holding coil, HC, was made of 3 m of 0.8 mm i.d. Teflon (PolyTetraFluoroEthylene, PTFE) tubing. The tubing connecting RV to the flow cell was 10 cm long, made of 0.8 mm i.d. PTFE tubing. The mixing coil, MC, was made of 25 cm of 2 mm i.d. polyethylene tubing. All other tubing connections were made of 0.8 mm i.d. PTFE tubing and PTFE nuts and ferrules (Upchurch, Oak Harbor, WA). An auxiliary peristaltic pump (not shown in Fig. 1) was used to continuously draw off the excess of solution inside the glass three-electrode cell, as previously described [23].

All reagents were of analytical grade and the working solutions were prepared in deionized water (Simplicity 185 system from Millipore coupled to an UV lamp). Stock 1000 mg L^{-1} standard solutions of Cu(II), Cd(II) and Pb(II) were bought from Carlo Erba and properly diluted with deionized water.

2.9. Copper, lead and cadmium adsorption measurements

A mass of 1.00 g of FDU-1 or FDU-1/HA_{15} suspension was dispersed in approximately 50 mL of deionized water. The pH was adjusted to 6.0 ± 0.1 with 0.050 mol L^{-1} NaOH solution and 5.00 mL of 0.1 mol L^{-1} 2-[*N*-morpholine]-ethanesulfonic acid (MES, pK_a 6.15) with pH 6.0,was added, being the volume adjusted to 100.0 mL with deionized water. Afterward, 2.50 mL aliquots of the buffered homogenized suspension were transferred to polypropylene centrifuge tubes with capacity of 15 mL. The final volume was adjusted to 5.00 mL with increasing volumes of 100 μmol L^{-1} stock solution of the individual studied cation and enough volume of deionized water, in order to obtain the metal cation concentrations: 5.0, 7.5, 10, 20, 30, 40 and 50 μmol L^{-1}. In all tubes the sorbent concentration in the suspensions was 10.0 g L^{-1}, in presence of 2.5 mmol L^{-1} of the MES buffer.

In another set of experiments a similar procedure was used, but with the stock solution containing a mixture of the three metal cations, each one at the concentration of 100 μmol L^{-1}. A blank experiment was carried out in parallel for each sample. All tubes were closed and maintained under gentle shaking for 24 h. After this time the pH was adjusted to 6.0 ± 0.1, if necessary. The tubes were centrifuged at 2600*g* for 15 min, and the supernatant solutions were stored for further determination of the free concentrations of the metal cations. The voltammetric determination was made with the sample solutions conditioned in 50 mmol L^{-1} acetic acid–sodium acetate buffer adjusted to pH 4.7 and 0.20 mol L^{-1} KCl as supporting electrolyte.

2.10. SIA procedure

The SIA operations are based on the scheme shown in Fig. 1. Initially, the HC and the electrochemical cell (Fig. 1) were filled with the carrier solution (C) (50 mmol L^{-1} acetic acid–sodium acetate buffer with pH 4.7 in 0.20 mol L^{-1} KCl). The tubing connecting the port 1 of RV was filled with standard (SD) or sample (S) solutions (SD or S). All the solutions used in the SIA system and in the electrochemical cell were previously de-aerated with ultra-pure N_2 to remove dissolved O_2. The potentiostat and the SIA programs were started simultaneously [33,34], but the potentiostat is programmed with a delay time of 22 s before applying the deposition potential (−0.8 V). During this time, with the syringe valve (SV) at position "OUT" (Fig. 1), the syringe pump aspirated 400 μL of C inside the syringe at a flow rate of 300 μL s^{-1}. Next, with SV at position "IN", 100 μL of air and 800 μL

of standard/sample solution were sequentially aspirated to HC at 50 μL s^{-1} from ports 8 and 1 of RV, respectively. Then, RV switched to port 3 and the syringe pump (SP) dispensed 700 μL of standard/sample toward the flow cell at 10 μL s^{-1}, while the potentiostat held the potential constant at −0.8 V for 80 s to perform the reduction (and concentration) of the metal cations in the Hg drop. The excess of sample/standard solution and the air bubble were expelled from HC dispensing 300 μL through port 6 of RV at a flow rate of 200 μL s^{-1}. Finally, RV switched back to port 3 and SP emptied the syringe at 100 μL s^{-1} performing the medium exchange so that the stripping step could be made in presence of the 50 mmol L^{-1} acetic acid–sodium acetate buffer in 0.20 mol L^{-1} KCl. The stripping step was made by the square wave mode of potential application and current reading, using a frequency of 100 Hz and pulse height of 25 mV. The calibration curves were constructed with standards of the metal cations at the concentrations 0, 0.25, 0.50, 1.0, 2.5, 5.0 and 10 μmol L^{-1}. The standard and sample solutions were prepared in 50 mmol L^{-1} acetic acid–sodium acetate buffer (pH 4.7) in 0.20 mol L^{-1} KCl.

2.11. Data treatment

Adsorption data were treated by the linearized Freundlich equation:

$$\log(q) = \log K_f + \left(\frac{1}{n}\right)\log[M^{2+}]$$

where q is the concentration of the studied compound in the solid phase (μmol g^{-1}), $[M^{2+}]$ is the solution concentration (μmol L^{-1}) after a given contact time (24 h in the present study), and K_f and $1/n$ are empirical constants related to adsorption.

3. Results and discussion

The TG/DTG curves of the samples are shown in the Fig. 2a–e and Δm, temperature range and Tpeak DTG curves are presented in the Table 1. The TG/DTG curves [Fig. 2a] indicated that the thermal composition process

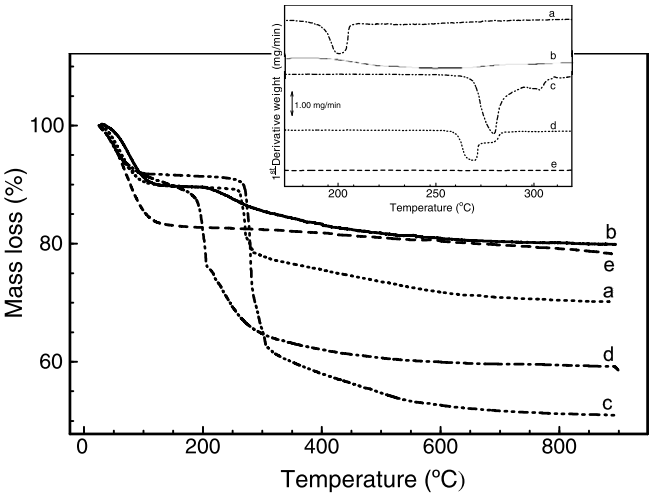

Fig. 2. TG curves for as-synthesized FDU-1 and FDU-1/ HA_{15} samples.

of FDU-1AS sample occurred in four mass loss steps (Table 1). The first step is due to the release of physically adsorbed water, the second and third steps correspond to template elimination and fourth mass loss is due to dehydroxilation step (transformation of silanols groups to siloxanes). For FDU-1EX sample, TG/DTG curves (Fig. 2b) indicate that the thermal decomposition process of template occur in only one mass loss step because the amount of template in this sample is smaller due to liberation of the larger part during the extraction process by solvent. The physically adsorbed water elimination and dehydroxilation steps were similar observed them for FDU-1AS sample. In the case of FDU-1/HA15AS sample the TG/DTG curves (Fig. 2c) evidence five mass losses steps (Table 1) and $\Delta m2$, $\Delta m3$ and $\Delta m4$ values correspond to thermal decomposition of template and humic acid modified in the material. The $\Delta m1$ and $\Delta m5$ corresponding to, respectively, the physically adsorbed water elimination and dehydroxilation steps. For FDU-1/HA15EX sample TG/DTG curves (Fig. 2d) evidence two mass losses steps for thermal decomposition of template and humic acid ($\Delta m2$ and $\Delta m3$) because the amount of template in this sample is smaller due to liberation of the larger part during the extraction process. The steps of physically adsorbed water elimination

Table 1
TG/DTG data for FDU-1 calcined, as-synthesized /extracted FDU-1 and FDU-1/HA_{15} samples

Samples	H_2O		Thermal decomposition of template/Humic acid and dehydroxilation							
	Δm_1 (%) [TR (°C)]	T_p (°C)	Δm_2 (%) [TR (°C)]	T_p (°C)	Δm_3 (%) [TR (°C)]	T_p (°C)	Δm_4 (%) [TR (°C)]	T_p (°C)	Δm_5 (%) [TR (°C)]	T_p (°C)
FDU-1 AS	10.7 [26 – 162]	51	14.4 [162 – 217]	201	15.0 [218 – 601]	231	0.7 [601 – 885]	874	–	–
FDU-1 EX	10.5 [29 – 170]	77	8.3 [170 –540]	247	1.5 [540 – 890]	562	–	–	–	–
FDU-1/ HA15AS	8.3 [25 – 166]	60	25.3 [166 – 297]	279	6.4 [297 – 354]	302	7.1 [354 – 599]	578	1.7 [599 – 900]	807
FDU-1/ HA15EX	10.4 [26 – 178]	64	12.6 [178 – 327]	269	5.8 [328 – 647]	398	1.1 [647 – 883]	674	–	–
FDU-1 calcined	17.2 [25 – 178]	74	4.4 [178 – 875]	578	–	–	–	–	–	–

T_p, peak temperature of DTG curve; TR, temperature range of TG event.

and dehydroxilation were similar observed them for FDU-1HA15AS sample. The comparison between DTG curves (inserted in Fig. 2) of the four samples, it evidences clearly that thermal decomposition process of template with humic acid occurs in temperatures larger, according to indicated by temperature peak of the DTG curves (*T*peak DTG). The TG/DTG curves of FDU-1 calcined sample (Fig. 2e) present only two mass losses. The first step is due to the release of physically adsorbed water and second mass loss is corresponding to dehydroxilation step. The solvent extraction process is not as efficient as calcinations, in removing templating but it is useful when the as-synthesized mesoporous materials have a organic–inorganic hybrid composite [35] as in the case of ordered mesoporous silica modified with HA (FDU-1/HA_{15} AS). In this case, thermogravimetric data showed that solvent extraction process had only partial efficiency, recovering only of 74.3% for FDU-1 EX and 49.1% for FDU-1/HA_{15} EX samples.

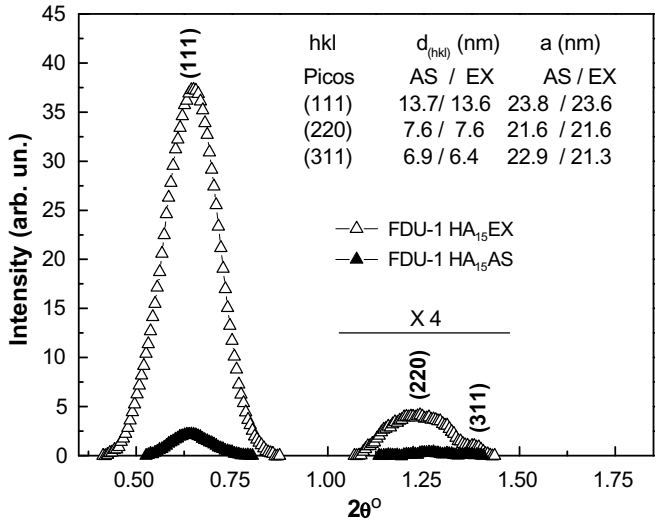

Fig. 3. Small angle X-ray diffraction (SAXRD) patterns for FDU-1AS and FDU-1EX.

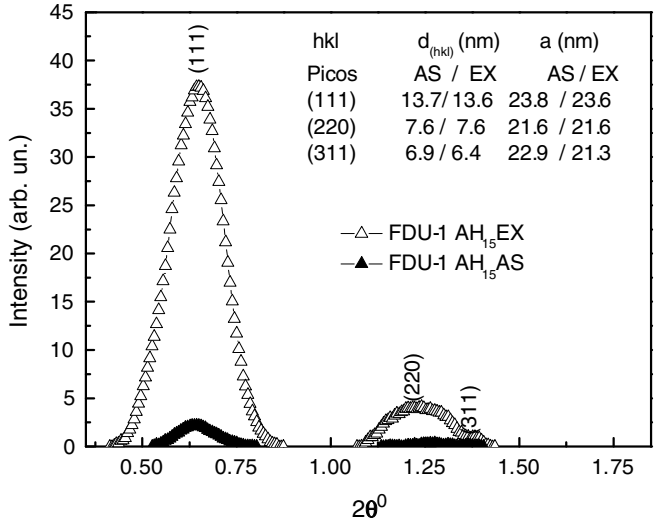

Fig. 4. Small angle X-ray diffraction (SAXRD) patterns for FDU-1/HA_{15}AS and FDU-1/HA_{15}EX.

Small angle X-ray diffraction patterns (SAXRD) for FDU-1AS, FDU-1EX are shown in Fig. 3 and FDU-1/HA_{15}AS, FDU-1/HA_{15}EX are shown in Fig. 4. The SAXRD data of the FDU-1 and FDU-1/HA15 samples showed reflections that are indexed as (1 1 1), (2 2 0) and (3 1 1) of the face-centered diamond cubic (fcc) structure. SAXRD patterns of these samples were quite similar to the ones reported earlier for FDU-1, synthesized by hydrothermal treatment with conventional heating [21] and microwave oven [22].

Wide angle X-ray diffraction data of our samples (not shown) confirmed the amorphous nature of silica walls, usually found in ordered mesoporous materials [21].

The SAXRD results show that the copolymer extraction with solvent does not induce a shrinkage of the structure as observed in usual calcination processes [1,2,14,15], therefore, it is a more adequate process for template removal.

The small angle diffracted intensity of the silica with copolymer and HA inside the pores is lower due to the presence of material inside the pores. The extraction of polymer (and HA) from the inner part of the pores increases the electronic contrast between the silica walls and the open space of the ordered pores, thus, increasing the diffracted intensity. But the intensity of FDU-1/HA_{15}EX is practically half the intensity of pristine FDU-1 EX (see intensity axis), evidencing the presence of matter around the pore walls, even after the solvent extraction process. This compound can be associated to HA, as supported by TG/DTG analysis.

Nitrogen adsorption isotherms of the extracted FDU-1 silica and the FDU-1/HA_{15}EX sample are shown in Fig. 5a and b. Both samples exhibited a high degree of structural ordering, as inferred from the steepness of the capillary condensation step on the adsorption isotherms. FDU-1 exhibited a high BET specific surface area of 515 $m^2 g^{-1}$, a total pore volume of 0.56 $cm^3 g^{-1}$ and FDU-1/HA_{15} exhibited a BET specific surface area of 457 $m^2 g^{-1}$, a total pore volume of 0.79 $cm^3 g^{-1}$; their adsorption capacity and the position of the capillary condensation step were similar to those commonly observed for FDU-1 EX and FDU-1/HA_{15}EX [16]. The steep capillary condensation steps at relative pressure of approximately 0.8 indicate uniformity of pore sizes. A comparison between FDU-1 EX and FDU-1/HA_{15}EX data shows that HA improves the materiaś properties, since the adsorption capacity, pore volume and pore wall thickness increase. The observed broad hysteresis loop, which closes at a relative pressure of approximately 0.45, is characteristic of cage-like mesoporous materials such as FDU-1 silica, having a large difference between porés diameter and their entrances [18–22]. Nitrogen adsorption isotherms for the FDU-1 and FDU-1/HA_{15} as-synthesized and extracted are shown in Fig. 5, whereas selected

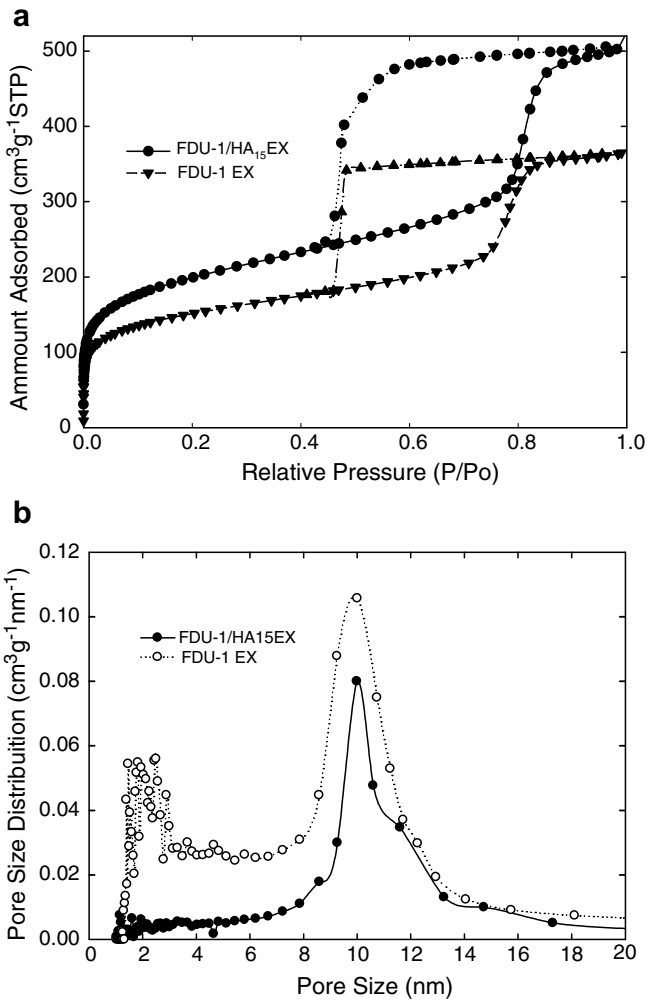

Fig. 5. Nitrogen adsorption isotherms at 77 K (a) and the corresponding pore size distributions (b) for the extracted FDU-1 and FDU-1/HA_{15} samples.

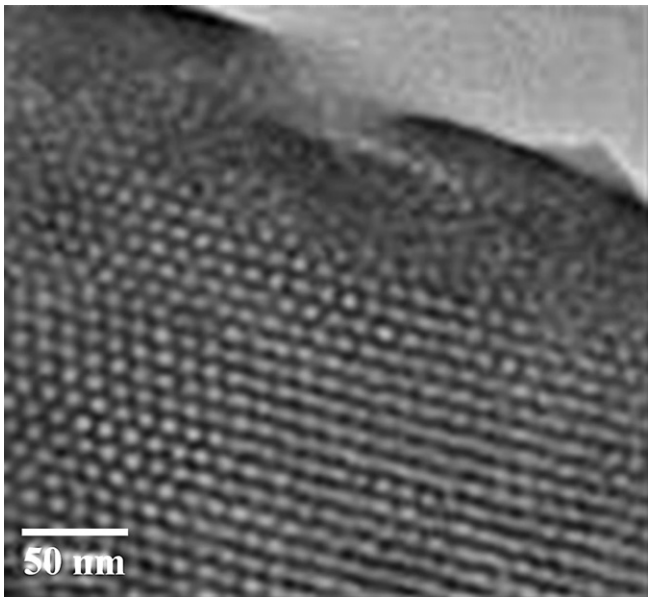

Fig. 6. Transmition electron microscopy image of FDU-1/HA_{15}EX sample.

structural parameters are listed in Table 2. In addition, FDU-1/HA_{15}EX was studied by high resolution transmission electron microscopy (HRTEM). The HRTEM micrograph in Fig. 6 reveals that the FDU-1/HA15EX possesses a high symmetric cubic mesoporous arrangement.

Fig. 7 shows the adsorption percentages as a function of the initial metal cation concentrations on both FDU-1EX (Fig 7a) and FDU-1/HA_{15}EX (Fig 7b). In the FDU-1EX the adsorption order is $Pb^{2+} > Cu^{2+} > Cd^{2+}$ for the low initial concentrations (5 and 10 μmol L^{-1}), but changed to $Pb^{2+} > Cd^{2+} > Cu^{2+}$ for concentrations higher than 10 μmol L^{-1}. The adsorption isotherms of Cd^{2+} and Cu^{2+} did not fit to Langmuir or Freundlich equations, contrary to Pb^{2+}, for which a typical L-type adsorption curve was obtained for the single and mixed cations solutions (Fig. 8). The Freundlich parameters for Pb^{2+} adsorption were $K_f = 2.3 \pm 0.1$ $\mu mol^{1-1/n}\, L^{1/n}\, g^{-1}$ and $1/n = 0.59 \pm 0.01$ ($r^2 = 0.998$).

At pH 6.0 the silanols are partially deprotonated, generating negatively charged SiO^- groups that can interact with the metal cations by electrostatic attractions, explaining the adsorption percentages observed in Fig. 7a. The affinity of the silanol by Pb^{2+} is greater than for Cu^{2+} and Cd^{2+}, a fact that may be explained by its greater ionic radius and smaller Z/R (charge/radius) ratio. As a consequence, Pb^{2+} creates a smaller electric field and will be less likely to remain solvated in face to competition for complexation with the silanols. Also in comparison to Cd^{2+} and Cu^{2+}, the larger radius of Pb^{2+} implies in larger spread of electron configuration in space and greater tendency to polarize in response to the electric field of the negative charges of the deprotonated silanols, increasing the tendency to form complexes. Additionally, the contribution of hydrolytic species such as $M(OH)^+$ is greater for Pb^{2+} than for Cu^{2+} and Cd^{2+}, a fact that can also explain the higher adsorption percentages of Pb^{2+}, because hydrolytic species are easier to dessolvate than the free metal cations [36,37]. These properties of Pb^{2+} explain its preferential adsorption and the small influence of competition in solutions containing the three metal cations. This is also supported by the Freundlich parameters for adsorption of Pb^{2+} onto FDU-1EX in presence of Cd^{2+} and Cu^{2+}, which were $K_f = 1.9 \pm 0.1$ $\mu mol^{1-1/n}\, L^{1/n}\, g^{-1}$ and $1/n = 0.52 \pm 0.05$ ($r^2 = 0.98$), and did not differ significantly from the ones obtained in absence of competition. The competition effect is strong for Cu^{2+}, especially at the highest concentration of 50 μmol L^{-1} of metal cations (Fig. 7a), a situation in which only about 22% of the initial Cu^{2+} was adsorbed on FDU-1EX.

Adsorption on FDU-1/HA_{15}EX was significantly enhanced in comparison to FDU-1EX (Fig. 7b), especially for Cu^{2+}. For the solutions containing only one heavy metal cation, the free concentration was smaller than that of the detection limit for Pb^{2+} and Cu^{2+} (0.09 and

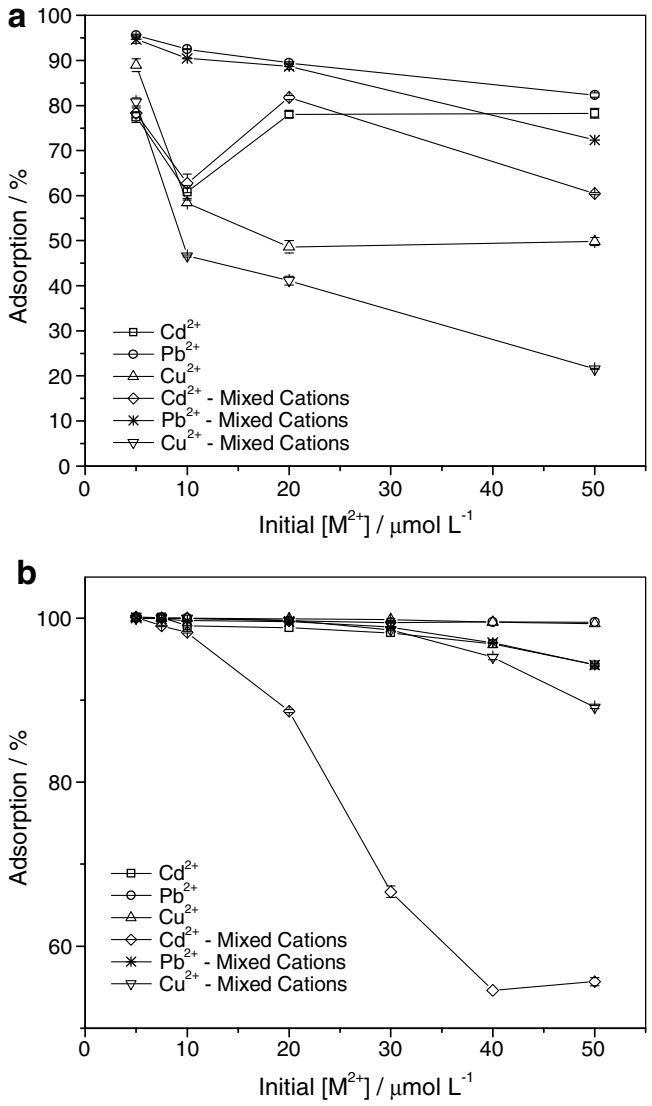

Fig. 7. Removal percentages of Cd^{2+}, Pb^{2+} and Cu^{2+} by adsorption on (a) FDU-1EX and (b) FDU-1/HA_{15}EX. The results are mean of two adsorption experiments.

0.16 μmol L^{-1}, respectively) up to the initial concentration of 10 μmol L^{-1}, implying in adsorption percentages greater than 99.1 % for Pb^{2+} and 98.4% for Cu^{2+}. For Cd^{2+}, the free cation concentration was smaller than that of the detection limit (0.06 μmol L^{-1}) for the two first points of the adsorption isotherm, allowing one to estimate adsorption percentages greater than 99.4% for initial concentrations $\leqslant$7.5 μmol L^{-1}.

The adsorption curves of metal ions on FDU-1/HA_{15}EX indicate a strong interaction between adsorbent and adsorbate (Figs. 8a and b). The experiments made with the three metal cations mixed in solution evidenced the competition for the adsorption sites between Cu^{2+} and Pb^{2+} only at initial concentrations of 40 and 50 μmol L^{-1} (Fig. 7b). Cadmium ions, on the other hand, are strongly affected by competition with the other two cations, and the removal percentages dropped markedly even for initial

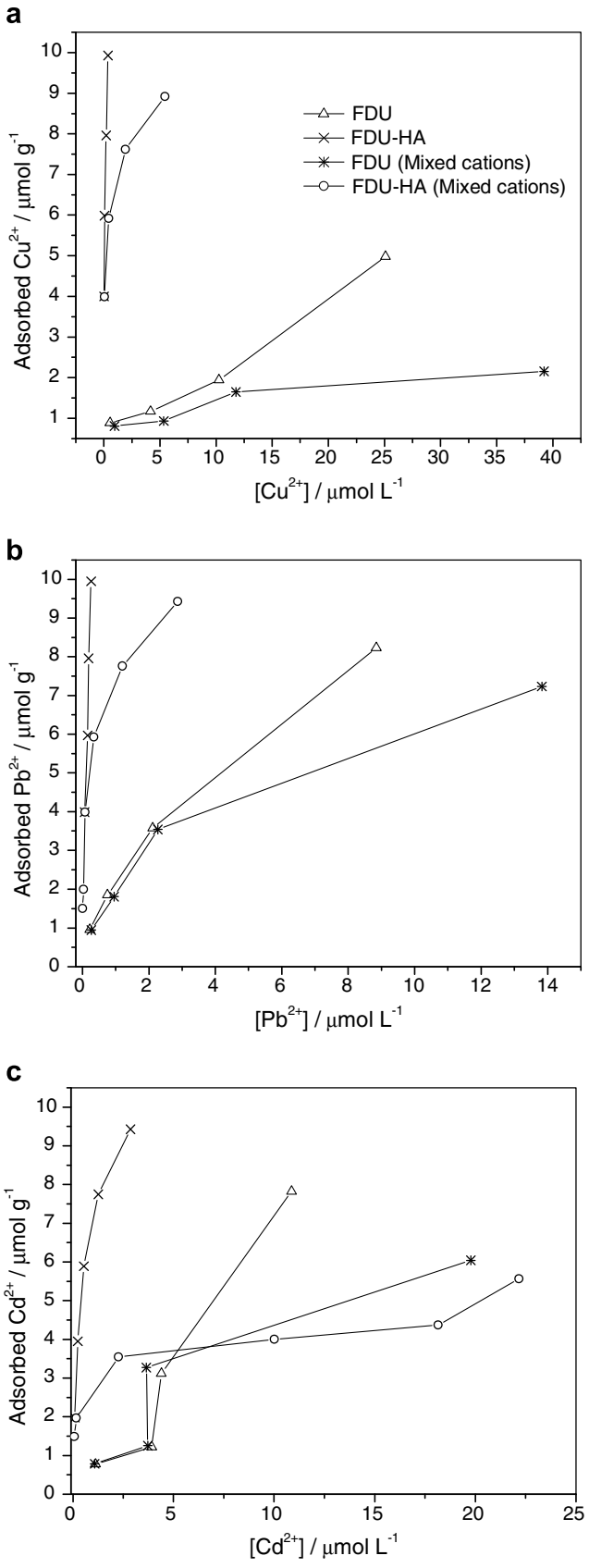

Fig. 8. Adsorption isotherms (25 ± 1) C of (a) Cu^{2+}, (b) Pb^{2+} and (c) Cd^{2+} on FDU-1EX and FDU-1/HA_{15}EX materials. Initial concentrations of the metal cations were between 5.0 and 50 μmol L^{-1}. The results are mean of two adsorption experiments.

Table 2
Structural and textural properties of FDU-1 and FDU-1/HA_{15} Samples

Sample	S_{BET} ($m^2\ g^{-1}$)	V_{pt} ($cm^3\ g^{-1}$)	V_M ($cm^3\ g^{-1}$)	V_m ($cm^3\ g^{-1}$)	w (nm)	$d_{(hkl)}$ (nm)	a (nm)	b (nm)
FDU-1 EX	515	0.56	0.47	0.09	10.0	13.9	24.1	5.3
FDU-1/HA_{15} EX	457	0.79	0.76	0.03	10.0	13.6	23.6	6.9

S_{BET}, BET specific surface area; V_{pt}, total pore volume; V_M, total mesopore volume; V_m, total micropore volume; w, primary mesopore diameter; $d_{(hkl),}$; lattice parameter ; a, unit-cell parameters; b, average pore wall thickness.

Table 3
Mean (± standard errors) Freundlich K_f ($\mu mol^{1-1/n}\ L^{1/n}\ g^{-1}$) and $1/n$ parameters for adsorption of Cd^{2+}, Pb^{2+} and Cu^{2+} onto FDU-1/HA_{15}EX

Adsorbate	K_f	$1/n$	r
Cd^{2+}	6.9 ± 0.3	0.35 ± 0.03	0.98
Pb^{2+}	25 ± 5	0.7 ± 0.1	0.98
Cu^{2+}	12.9 ± 0.6	0.29 ± 0.1	0.99
Cd^{2+} (mixed cations)	2.7 ± 0.1	0.20 ± 0.02	0.98
Pb^{2+} (mixed cations)	7.4 ± 0.7	0.32 ± 0.03	0.98
Cu^{2+} (mixed cations)	6.7 ± 0.3	0.18 ± 0.01	0.99

concentrations as low as 7.5 μmol L^{-1} (Fig. 7b and Fig. 8c).

The significant enhancement of adsorption of the metal cations on FDU-1/HA_{15}EX suggests a change in the adsorption mechanism in comparison to FDU-1 EX. The complexation with carboxylic and phenolic groups of the humic substance adsorbed to the silica is probably the major mechanism governing the adsorption of low concentrations of the metal cations on the FDU-1/HA_{15}EX material. This change of adsorption mechanism is especially important for Cu^{2+}, which among the studied cations is the one that forms the most stable complexes with humic substances [28,38]. Complexation of Cd^{2+} by humic substances is the weakest among the studied cations, and the enhancement of its adsorption on FDU-1/HA_{15}EX in single cation solution is almost completely lost in the experiment made in presence of Cu^{2+} and Pb^{2+} (Fig. 7). Adsorption percentages and K_f parameters (Table 3) show that the adsorption capacity order on FDU-1/HA_{15}EX is $Pb^{2+} \cong Cu^{2+} > Cd^{2+}$. The $1/n < 1$ Freundlich parameters also corroborate with chemisorption mechanism involving inner sphere surface complexes between humic substance groups and the metal cations, as well as with the high heterogeneity of adsorption sites. In these cases, a small number of adsorption sites with strong affinity by the metal cations govern adsorption at low degree of site occupation, but as the metal cation concentrations increase, these sites become saturated, and the silanols groups then govern the adsorption.

4. Conclusion

The TG/DTG data show that the incorporation of HA (FDU-1/HA_{15}) in silica wall structure increases the temperature of thermal decomposition of the template, which occurred at higher temperature than that in FDU-1. The SAXRD patterns show that the FDU-1 and FDU-1/HA_{15} samples present F$m3m$ diamond face-centered cubic (fcc) structure and indicate that the incorporation of HA is inside the pores. Nitrogen adsorption isotherms showed that structural properties of FDU-1 EX and FDU-1/HA_{15}EX led to a substantial improvement of the BET specific surface area, total pore volume and wall thickness. Incorporation of humic acid into the mesopores of FDU-1 material afforded an adsorbent with strong affinity for Cd^{2+}, Cu^{2+} and Pb^{2+} from single ion solutions. On the other hand, in mixed cation solutions, competition by the adsorption sites is likely to occur and, in this situation, the adsorption preference is for Pb^{2+} and Cu^{2+}. Adsorption of Cu^{2+} was significantly enhanced after incorporation of humic acid, a fact that can be explained by formation of complexes with carboxylic and phenolic groups at low concentrations of the metal cation. FDU-1/HA_{15}EX has potential applicability in the removal of low concentrations of heavy metal cations from aqueous solution, such as wastewaters, after usual precipitation of metal hydroxides in alkaline medium and proper pH conditioning in the range between 6 and 7. Higher pH values would imply in chemical attack to silica structures and desorption of humic acid.

Acknowledgements

Thanks are due to FAPESP (L.C. Cides da Silva, Grants 03/10067-3), CNPq and CAPES, for financial support. The authors thank Prof. Elizabeth de Oliveira from LEEAA/IQ-USP and Mr. Wilson Hernandes from Anacom Científica (commercial representative of Milestone Inc at Brazil) for the use of the microwave oven. The authors thank LME/LNLS for technical support during electron microscopy work.

References

[1] C.T. Kresge, M.E. Leonowicz, W.J. Roth, J.C. Vartuli, J.S. Beck, Nature 359 (1992) 710.
[2] J.S. Beck, J.C. Vartuli, W.J. Roth, M.E. Leonowicz, C.T. Kresge, K.D. Schmitt, C. T-W. Chu, D.H. Olson, E.W. Sheppard, S.B. McCullen, J.B. Higgins, J.L. Schlenker, J. Am. Chem. Soc. 114 (1992) 10834.
[3] T. Yanagisawa, T. Shimizu, K. Kuroda, C. Kato, Bull. Chem. Soc. Jpn. 63 (1990) 988.
[4] S. Inagaki, Y. Fukushima, K. Kuroda, J. Chem. Soc., Chem. Commun. (1993) 680.
[5] A. Sayari, Chem. Mater. 8 (1996) 1840.
[6] A. Corma, Chem. Rev. 97 (1997) 2373.
[7] G.J. de A.A. Soler-Illia, C. Sanchez, B. Lebeau, J. Patarin, Chem. Rev. 102 (2002) 4093.

[8] S. Polarz, M. Antonietti, Chem. Commun. (2002) 2593.
[9] A.P. Wright, M.E. Davis, Chem. Rev. 102 (2002) 3589.
[10] D.E. De Vos, M. Dams, B.F. Sels, P.A. Jacobs, Chem. Rev. 102 (2002) 3615.
[11] Y. Liu, T.J. Pinnavaia, J. Mater. Chem. 12 (2002) 3179.
[12] A. Stein, Adv. Mater. 15 (2003) 763.
[13] T. Linssen, P. Cassiers, E.F. Vansant, Adv. Colloid Interface Sci. 103 (2003) 121.
[14] D. Zhao, Q. Huo, J. Feng, B.F. Chmelka, G.D. Stucky, J. Am. Chem. Soc. 120 (1998) 6024.
[15] D. Zhao, J. Feng, Q. Huo, N. Melosh, G.H. Fredrickson, B.F. Chmelka, G.D. Stucky, Science 279 (1998) 548.
[16] L.C.C. Silva, T.S. Martins, M. Santos Filho, E.E.S. Teotônio, P.C. Isolani, H.F. Brito, M.H. Tabacniks, M.C.A. Fantini, J.R. Matos, Micropor. Mesopor. Mater. 94 (2006) 92.
[17] L.C. Cides da Silva, G. Abate, N.A. Andrea, M.C.A. Fantini, J.C. Mazini, L.P. Mercuri, O. Olkhovyk, J.R. Matos, Studies Surf. Sci. Catal. 156 (2005) 941.
[18] C. Yu, Y. Yu, D. Zhao, Chem. Commun. (2000) 575.
[19] C. Yu, B. Tian, J. Fan, G.D. Stucky, D. Zhao, J. Am. Chem. Soc. 124 (2002) 4556.
[20] M. Kruk, E.B. Celer, M. Jaroniec, Chem. Mater. 16 (2004) 698.
[21] J.R. Matos, M. Kruk, L.P. Mercuri, M. Jaroniec, L. Zhao, T. Kamiyama, O. Terazaki, T.J. Pinnavaia, Y. Liu, J. Am. Chem. Soc. 125 (2003) 821.
[22] M.A.C. Fantini, J.R. Matos, L.C. Cides da Silva, L.P. Mercuri, G.O. Chiereci, E. Celer, M. Jaroniec, J. Eng. Sci. Mat. B 112 (2004) 106.
[23] G. Abate, J. Lichtig, J.C. Masini, Talanta 58 (2002) 433.
[24] D. Buerge-Weirich, R. Hari, H. Xue, P. Behra, L. Sigg, Environ. Sci. Technol. 36 (2002) 328.
[25] G. Abate, J.C. Masini, Colloids Surf. A 226 (2003) 25.
[26] C. Lai, C. Chen, B. Wei, S. Yeh, Water Res. 36 (2002) 4943.
[27] A. Liu, R.D. Gonzales, J. Colloid Interface. Sci. 218 (1999) 225.
[28] G. Abate, J.C. Masini, Quim. Nova 22 (1999) 661.
[29] S. Brunauer, P.H. Emmet, E. Teller, J. Am. Chem. Soc. 60 (1938) 309.
[30] E.P. Barret, L.G. Joyner, P.H. Halenda, J. Am. Chem. Soc. 73 (1951) 309.
[31] M. Kruk, M. Jaroniec, A. Sayari, Langmuir 13 (1997) 6267.
[32] P.I. Ravikovitch, A.V. Neimark, Langmuir 18 (2002) 550.
[33] L.B.O. dos Santos, M.S.P. Silva, J.C. Masini, Anal. Chim. Acta 528 (2005) 21.
[34] A.C.V. dos Santos, J.C. Masini, Anal. Bioanal. Chem. 385 (2006) 1538.
[35] S. Inagaky, S. Guan, T. Ohsuna, O. Terasaky, Nature 416 (2002) 304.
[36] G. Sposito, The Chemistry of Soils, Oxford University Press, New York, 1989.
[37] M.B. McBride, Environmental Chemistry of Soils, Oxford University Press, New York, 1994.
[38] G. Abate, J.C. Masini, J. Braz. Chem. Soc. 12 (2001) 109.